# Self-sustained oscillations with acoustic feedback in flows over a backward-facing step with a small upstream step

Hiroshi Yokoyama[a)]
*Graduate School of Engineering, The University of Tokyo, 7-3-1 Hongo, Bunkyo-ku, Tokyo, 113-8656 Japan*

Yuichi Tsukamoto
*Hitachi Plant Technologies, Ltd., 4-5-2 Higashi-Ikebukuro, Toshima-ku, Tokyo, 170-8466 Japan*

Chisachi Kato
*Institute of Industrial Science, The University of Tokyo, 4-6-1 Komaba, Meguro-ku, Tokyo, 153-8505 Japan*

Akiyoshi Iida
*Faculty of Engineering, Kogakuin University, 2665 Nakano-machi, Hachioji-shi, Tokyo, 192-0015 Japan*

(Received 16 January 2007; accepted 6 September 2007; published online 23 October 2007)

Self-sustained oscillations with acoustic feedback take place in a flow over a two-dimensional two-step configuration: a small forward-backward facing step, which we hereafter call a bump, and a relatively large backward-facing step (backstep). These oscillations can radiate intense tonal sound and fatigue nearby components of industrial products. We clarify the mechanism of these oscillations by directly solving the compressible Navier-Stokes equations. The results show that vortices are shed from the leading edge of the bump and acoustic waves are radiated when these vortices pass the trailing edge of the backstep. The radiated compression waves shed new vortices by stretching the vortex formed by the flow separation at the leading edge of the bump, thereby forming a feedback loop. We propose a formula based on a detailed investigation of the phase relationship between the vortices and the acoustic waves for predicting the frequencies of the tonal sound. The frequencies predicted by this formula are in good agreement with those measured in the experiments we performed. © *2007 American Institute of Physics*. [DOI: 10.1063/1.2793170]

## I. INTRODUCTION

Self-sustained oscillations with tonal sound, such as cavity tones or edge tones, frequently take place when solid bodies are placed in shear layers. These oscillations are described as fluid-acoustic interactions and are interesting phenomena both for aerodynamics and for aeroacoustics. Moreover, the prediction and the suppression of the oscillations are very important for many practical applications. When the oscillations are unsuppressed, the noise levels in open cavities in aircraft can exceed 150 dB.[1] These intense oscillations can fatigue nearby components such as aircraft wheel-wells and landing-gear configurations.[2]

For decades, many researchers have used various approaches to investigate the relationship between the flow and the sound in these phenomena. Brown[3] experimentally found that the peak frequencies of the edge tones change discontinuously against the position of the edge and the mean flow velocity. Powell[4] proposed that the interactions of vortices in a jet with a sharp edge generate acoustic waves that lead to the formation of new vortices, and the frequencies predicted by his proposal agree well with Brown's experimental results.[3] Meanwhile, Rossiter[5] proposed a similar feedback loop over open cavities and derived a semiempirical formula, $fL/u_0=(n-\gamma)/(M+1/\kappa)$, where $f$ is the frequency of the radiated tonal sound, $L$ is the cavity length, $u_0$ is the free stream velocity, $n$ is a positive integer, $M$ is the Mach number based on the free stream velocity, $\kappa$ is the ratio of the convection velocity of vortices to the free stream velocity, and $\gamma$ is a constant for the phase correction. The frequencies predicted by this formula agree with those measured in experiments.[6] However, this model does not provide the values of $\kappa$ and $\gamma$ theoretically, treating them instead as empirical constants to be determined by the best fit with measured data.

In theoretical studies, the shear layer was idealized as a vortex sheet, and the phase distributions of the vortices and the sound were estimated for edge tones, cavity tones, and aperture tones. The results enabled researchers to predict the frequencies of the tonal sound without using empirical or adjustable parameters (Bilanin and Covert,[7] Tam and Block,[8] Crighton,[9] and Howe[10]). However, the phase distributions estimated by these studies have not been validated by experiments or computations. In recent years, the direct numerical simulation (DNS), where both vortices and acoustic waves are directly simulated, has provided a means of studying the self-sustained oscillation mechanism in detail[11,12] (see the review of Colonius and Lele[13]). However, few studies have been done about the detailed mechanism of vortex shedding and acoustic radiation, including the phase relationship between the vortices and the sound in the self-sustained oscillations. Therefore, the physical meaning of constant $\gamma$ in Rossiter's formula[5] remains unknown.

The self-sustained oscillations with tonal sound also take place in a flow over a two-step configuration: a small forward-backward facing step, which we hereafter call a

[a)]Electronic mail: yokoyama@iis.u-tokyo.ac.jp

 

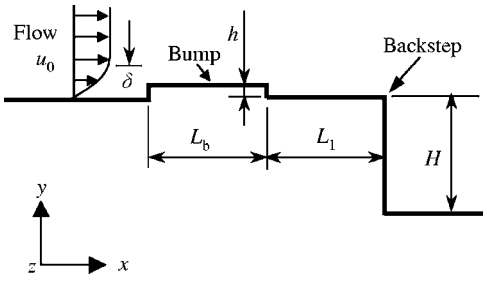


FIG. 1. Flow configurations.

bump, and a relatively large backward-facing step or backstep (Fig. 1). This configuration appears in various industrial devices, for example, the small bump on the surface of an automobile side mirror. The tonal sound caused by the oscillations is uncomfortable for the passengers, so the mechanism of the oscillations needs to be clarified so that the sounds can be predicted and reduced. However, few studies have been done on the self-sustained oscillations in this configuration, and there are many open questions about the formation of vortices around the bump and about the acoustic radiation. The objective of the present work is to answer these questions, focusing on the phase relationship between the vortices and the sound.

This work mainly consists of computational studies, but we also conducted wind-tunnel experiments to validate the computational results. In Sec. II, we explain the flow configurations, the numerical methods, and the experimental setup. In Sec. III A, we discuss the pressure fluctuation at a point far from the backstep and confirm that tonal sound is radiated. In Sec. III B, we present instantaneous vortices and acoustic waves in detail. In Sec. III C, acoustic sources are clarified. In Sec. III D, the phase relationship between the vortices and the acoustic waves are clarified. Based on this relationship, we propose a formula for predicting the frequencies of the radiated tonal sound in Sec. III E. The frequencies predicted by this formula are compared with those measured in the experiments that we performed.

## II. METHODOLOGY

### A. Flow configurations

The baseline flow configurations and parameters for the present work are shown in Fig. 1 and Table I, respectively. The bump is placed in a laminar boundary layer. The Reynolds number $\mathrm{Re}_x$ based on the value of $x$ measured from the virtual origin is $4.6\times10^5$ at the leading edge of the bump. Mach number $M$ based on free-stream velocity $u_0$ is 0.088 in the experiments, but in the computations we investigate the flow with higher Mach numbers $M=0.3$, 0.4, and 0.5 to reduce the computational costs.

TABLE I. Parameters.

| Boundary layer | $\mathrm{Re}_x$ | $L_b/h$ | $L_1/h$ | $\delta/h$ | $H/h$ |
|---|---|---|---|---|---|
| Laminar | $4.6\times10^5$ | 14.3 | 14.3 | 2.4 | 21.6 |

Boundary layer thickness is 2.4 $h$ at the leading edge of the bump, and bump length $L_b$ is 14.3 $h$, where $h$ is bump height. Distance $L_1$ between the trailing edge of the bump and that of the backstep is 14.3 $h$. We have clarified in preliminary experiments that intense tonal sound is radiated from the flow with these configurations. Backstep height $H$ is 21.6 $h$ in the computations and 71.4 $h$ in the experiments. In the computations, the flow fields are developed more quickly by shortening backstep height, which also determines the necessary streamwise length of the computational domain. To clarify the effect of backstep height on the mechanism of the self-sustained oscillations, we compare the computational results of the baseline configurations with those where backstep height $H$ is 43.1 $h$ in Sec. III E.

### B. Numerical methods

#### 1. Governing equations

We simulate both flow and acoustic fields by directly solving the three-dimensional compressible Navier-Stokes equations in a conservative form, which are written as

$$U_t + (E - E_v)_x + (F - F_v)_y + (G - G_v)_z = 0, \tag{1}$$

where $U$ is the vector of the conservative variables, $E$, $F$, and $G$ are the inviscid fluxes, and $E_v$, $F_v$, and $G_v$ are the viscous fluxes. The spatial derivatives are evaluated by the sixth-order-accurate compact finite difference scheme (fourth-order accurate on the boundaries).[14] Time integration is performed by a third-order accurate Runge-Kutta method. To suppress the numerical instabilities associated with the central differencing in the compact scheme, we use the tenth-order-accurate spatial filter shown below,[15]

$$\alpha_f\hat{\phi}_{i-1} + \hat{\phi}_i + \alpha_f\hat{\phi}_{i+1} = \sum_{n=0}^{5}\frac{a_n}{2}(\phi_{i+n} + \phi_{i-n}), \tag{2}$$

where $\phi$ is a conservative quantity and $\hat{\phi}$ is the filtered quantity. Coefficients $a_n$ are the same as the values used by Gaitonde and Visbal,[16] and parameter $\alpha_f$ is 0.45. We have clarified in preliminary tests that we can capture acoustic waves by 10 points per wave (ppw) using the above computational methods.

#### 2. Computational grid

To evaluate the effect of the three-dimensional distortion of relatively large vortices in the wake of the backstep on the radiated sound, we use a three-dimensional computational grid for the present simulations (Fig. 2). The spanwise extent of the computational domain is $L_z=3H$, and the cross section in the $x$-$y$ plane is shown in Fig. 3. We use 11 grids in the spanwise direction and investigate grid dependence by changing the number of the grids in the spanwise direction in Sec. III A. The grid resolution we used for acoustic propagation was more than 40 grids per wavelength of the fundamental frequency to suppress the dissipation of the acoustic waves, and 11 grids per bump height $h$ so that small flow structures generated by the bump can be captured. The present computational domain consists of approximately $2.5\times10^5$ structured grids.

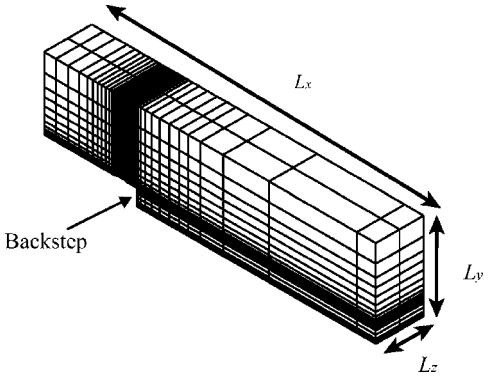


FIG. 2. Computational grid (every fifth grid line is shown for clarity).

### 3. Initial conditions, boundary conditions, and buffer zone

All the simulations were initiated by the uniform flow with free-stream velocity $u_0$ over the bump and the backstep.

Figure 3 shows the boundary conditions used in the present studies. The artificial boundaries must allow vortices and acoustic waves to pass smoothly with minimal disturbances. In this study, the nonreflecting boundary conditions based on the characteristic wave relations[17–19] are used at the inflow, upper, and outflow boundaries. Nonslip and adiabatic boundary conditions are used at the wall. The periodic boundary conditions are used in the spanwise direction.

To minimize errors associated with the artificial boundaries, buffer zones (where we stretch the grid to reduce the amplitudes of the acoustical and vortical fluctuations before they reach the boundaries) are used near the nonreflecting boundaries. Moreover, we must keep boundary layer thickness $\delta$ constant at the leading edge of the bump because the radiated sound strongly depends on the boundary layer thickness. To achieve desired thickness $\delta$ at the leading edge of the bump, Eq. (1) is replaced in the upstream buffer zone by

$$U_t + (E - E_v)_x + (F - F_v)_y + (G - G_v)_z = -\sigma_0 (a/L_b)\xi^2 (U - U_{\text{target}}), \tag{3}$$

where $\sigma_0$ is 0.05, $a$ is the speed of sound, $L_b$ is the length of the buffer zone, $\xi$ is the nondimensional distance from the beginning of the buffer zone to the inflow boundary ($0 \leqslant \xi \leqslant 1$), and $U_{\text{target}}$ is the target vector of the conservative variables.[20,21] $U_{\text{target}}$ is obtained from the calculation for the flat-plate laminar boundary layer.

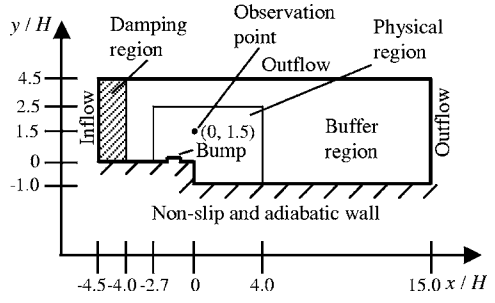


FIG. 3. Boundary conditions.

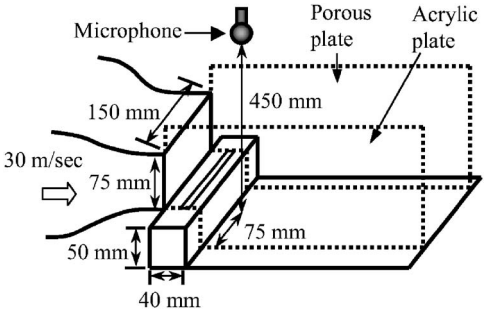


FIG. 4. Experimental setup.

### C. Experimental setup

We conducted our experiments using the suction-type low-noise wind tunnel shown in Fig. 4. The test section is composed of a backstep accompanied by a small bump placed upstream of the backstep. In the spanwise direction, the test section is terminated by two end walls. One of these walls is made of a porous plate to suppress the reflections of the sound, and the other is made of an acrylic plate, which allows optical observations. The velocity profile and the sound pressure level are measured, respectively, with a hot wire anemometer and a sound level meter with a nondirectional 1/2 in. microphone (Rion NL-31).

At a wind speed of 30 m/s, the turbulence intensity is less than 0.7% and the nonuniformity of the mean flow velocity is less than 0.1%. The velocity profile at the point of the leading edge of the bump is measured without the bump. The profile agrees with the Blasius profile, so the boundary layer is apparently laminar (Fig. 5). At a wind speed of 30 m/s, the 99% boundary layer thickness, the momentum thickness, the displacement thickness, and the shape factor are 1.7 mm, 0.23 mm, 0.58 mm, 2.6, respectively. The test section is placed in an anechoic chamber that is covered with 50 mm thick sound-absorbing material, and the background noise level is suppressed to less than 64 dB at a wind speed of 30 m/s, which is much lower than the sound pressure level of the tonal sound of our interest.

To account for errors and uncertainties, we estimated that the error of the measurement of the streamwise velocity is 0.2 m/s at a wind speed of 30 m/s and that of the bump height is 0.1 mm. We found that the uncertainty about the

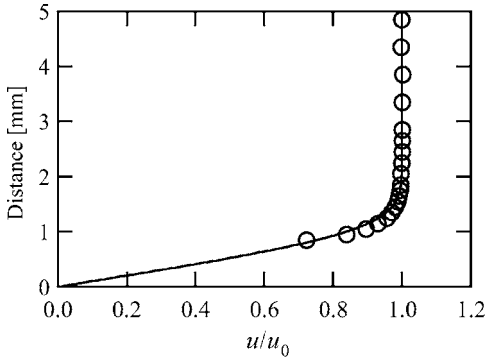


FIG. 5. Velocity profile of boundary layer. Measured data (○) is compared with the Blasius profile (—).

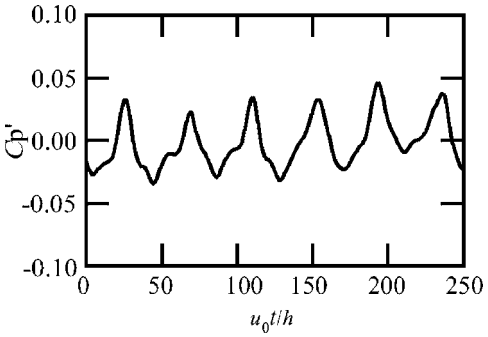


FIG. 6. Fluctuation of pressure coefficient *Cp* at the observation point shown in Fig. 3.

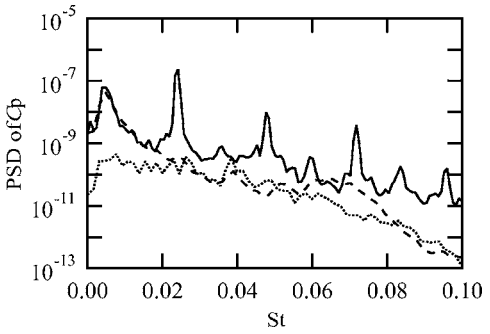


FIG. 8. Power spectrum density of pressure coefficient *Cp* for baseline configuration (—) compared with a simple backstep without a bump (---) and a bump on a flat plate without a backstep (···).

peak frequency of the tonal sound is about 40 Hz when the peak frequency is 2370 Hz. To evaluate the repeatability of the experiments, we repeated the experiments and measured the frequency spectra 10 times at a frequency resolution of 10 Hz. We found that the 95% uncertainty range of the peak frequency of the radiated sound was 24 Hz.

## III. RESULTS AND DISCUSSION

### A. Self-sustained oscillations with tonal sound

Figure 6 shows the fluctuation of the pressure coefficient $Cp$ $[=p/(\rho_0 u_0^2/2)]$ for $M=0.4$, where $\rho_0$ is the density of the ambient air at the observation point (Fig. 3) after 20 flow-through times have elapsed since the start of the computation. This shows that the flow is fully developed from the initial condition and that the oscillations are occurring. We also investigated the oscillations when either the bump or the backstep had been removed (Fig. 7). Figure 8 shows a comparison of the frequency spectra of the pressure fluctuations at the observation point. We averaged the results of the Fourier transform 20 times and the duration of the transform is about 1300 $(h/u_0)$. This duration corresponds to about 30 periods of the fundamental mode. The results clearly indicate that the tonal sound with the fundamental frequency $\mathrm{St}=fh/u_0=0.024$ is radiated only when both the bump and the backstep exist. We also found that the fundamental frequencies of the tonal sound are St=0.025 and 0.023, respectively, for $M=0.3$ and 0.5 for the baseline configuration. We investigated the effect of the grid resolution and the width of the computational domain by conducting the computations with 21 grids over $Lz=3H$ (the original width) and $Lz=6H$ for $M=0.4$. Figure 9 shows that the frequency spectra do not change from that of the original spectrum. Therefore, we concluded that the original resolution and width are sufficient to capture the effect of the distortion of the large vortices in the wake of the backstep on the radiated sound.

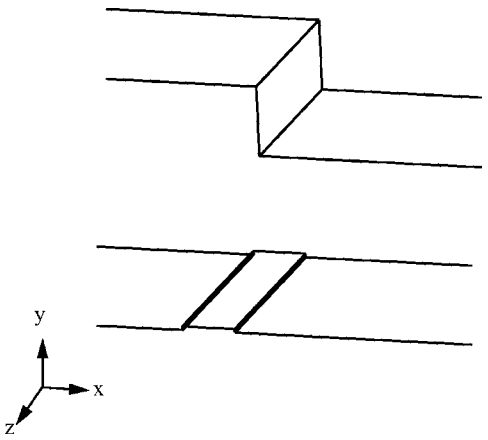


FIG. 7. Configurations without bump (top) and without backstep (bottom).

### B. Instantaneous distributions of vortices and acoustic waves

We investigated the vortical structures and the acoustic fields in oscillations when the flow is fully developed from the initial condition. To elucidate the flow structures, the second invariant of the velocity gradient tensor $Q=\|\Omega\|^2-\|S\|^2$ was computed, where $\Omega$ and $S$ are, respectively, the antisymmetric and symmetric parts of the velocity gradient tensor. Regions with $Q>0$ represent vortex tubes. We present the acoustic fields using density fluctuations. Using these methods of visualization, we were able to clearly capture the flow structures and the acoustic waves in the near field. Figure 10 shows instantaneous flow structures and acoustic waves for $M=0.4$ from $t=0$ to $t=0.81T$, where $T$ represents the period of the fundamental frequency. A small vortex ("Vortex 3" at $t=0$) is shed from the leading edge of the bump and convected downstream. While being convected from the trailing edge of the bump to the backstep, the vortex merges with its

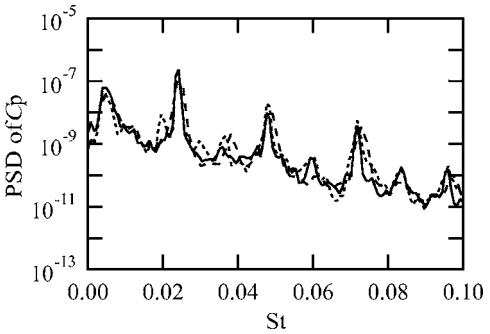


FIG. 9. Power spectrum density of pressure coefficient *Cp* for the original case of 11 grids over $Lz=3H$ (—) compared with the case of 21 grids over $Lz=3H$ (---) and with that of 21 grids over $Lz=6H$ (···).

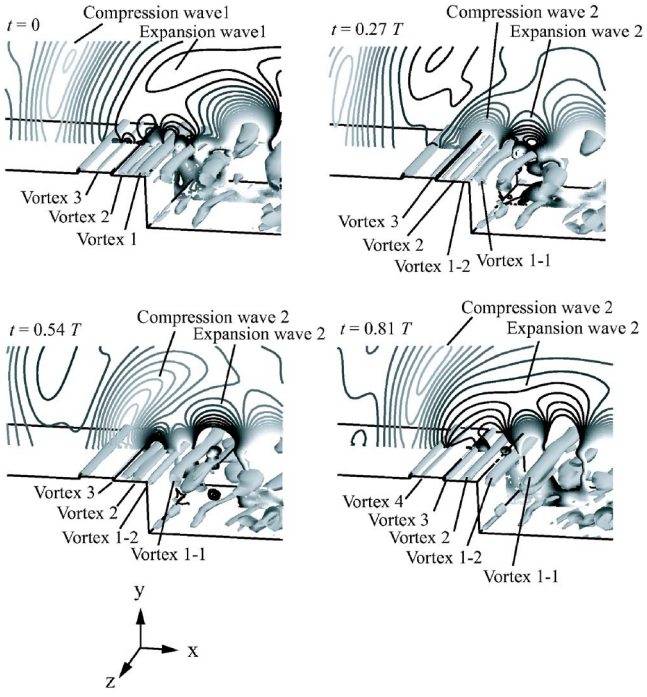


FIG. 10. Contours of density fluctuations $\rho'/\rho_0$ and isosurfaces of $Q/(u_0/\delta)^2=0.03$. Contour levels range from $-5\times10^{-3}$ (dark) to $5\times10^{-3}$ (light). "$T$" represents the period of fundamental frequency.

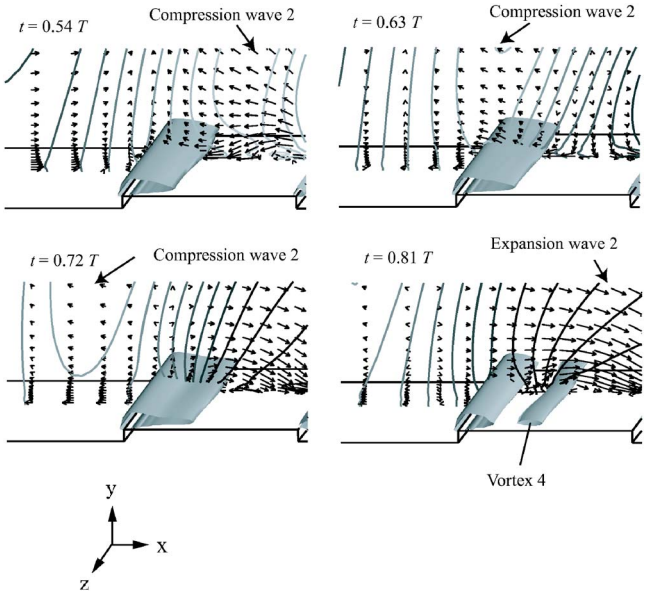


FIG. 12. Contours of density fluctuations $\rho'/\rho_0$ and isosurfaces of $Q/(u_0/\delta)^2=0.03$. Contour levels range from $-5\times10^{-3}$ (dark) to $5\times10^{-3}$ (light). Vectors represent fluctuations of velocity. "$T$" represents the period of fundamental frequency.

upstream vortex and becomes a larger vortex ("Vortex 2" at $t=0.54T$). When it passes the trailing edge of the backstep, the vortex splits into a fast vortex and a slow vortex ("Vortex 1-1" and "Vortex 1-2" at $t=0.27T$), and the convection velocity differs between the two vortices depending on the distance from the wall. A compression wave ("Compression wave 2" at $0.27T$) is radiated between this slow vortex and its upstream vortex. Meanwhile, an expansion wave ("Expansion wave 2" at $0.27T$) is radiated from the vortices distorted in the wake of the backstep. The behaviors of the acoustic wave fronts show that the acoustic waves are propagated in the upstream direction along the wall at a velocity of about $a$-$u_0$.

Figure 11 shows the trajectories of the vortices ($y=1.6\,h$) and those of compression waves ($y=3.6\,h$) represented by the local maxima of the second invariant and density, respectively. This figure shows that the shed of a vortex coincides

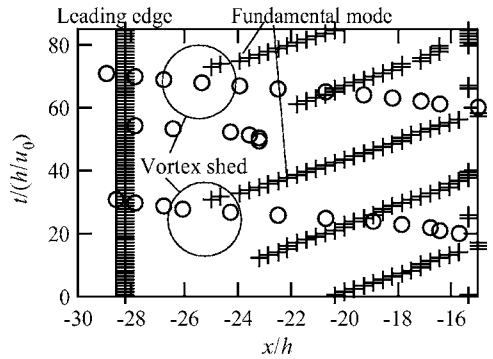


FIG. 11. Trajectories of vortices (+) and compression waves (○) over the bump.

with the crossing of the compression wave. Figure 12 shows the vortices and the acoustic waves around the leading edge of the bump from $t=0.54T$ to $t=0.81T$, including the vectors of velocity fluctuations. The velocity fluctuation virtually represents the sound particle velocity, although it is affected by the vortices near the wall. Due to acoustic expansion, the gradient of the sound particle velocity in the streamwise direction changes suddenly from a negative to a positive value just after the most compressed wave (local maximum line of density) passes. This is because the gradient of pressure fluctuation is very steep around the maximum point, as shown in Fig. 6. As a result, the vortex formed by the flow separation at the leading edge of the bump begins to stretch and finally a new vortex, "Vortex 4," is shed at $t=0.81\ T$ when the compression wave ("Compression wave 2") passes this vortex in the upstream direction. It also shows that there are trajectories of modes higher than the fundamental mode of St=0.24.

### C. Acoustic sources

To identify the source positions of the radiated tonal sound, we investigated the amplitudes of the pressure fluctuations for the fundamental frequency for $M=0.4$ (Fig. 13). The local maxima of the fluctuations appear in both the upstream and downstream regions of the backstep. The upstream local maximum represents the source of the compression waves radiated between the vortex at the trailing edge of the backstep and its upstream vortex ($t=0.27\ T$ in Fig. 10). The distance between this point and the trailing edge of the backstep is $L_\beta\approx3.6h$. The same value of $L_\beta$ is also obtained for $M=0.3$ and 0.5. This value is important for predicting the frequencies of the radiated tonal sound because the compression waves cause new vortices at the leading edge of the bump. Meanwhile, the local maximum downstream of the

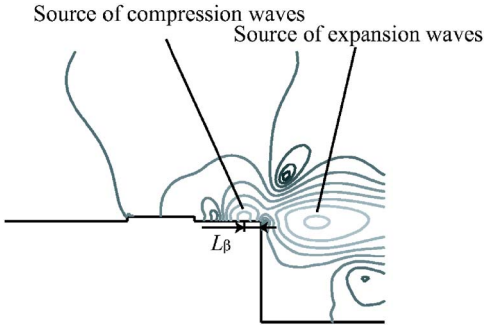


FIG. 13. Amplitudes of pressure coefficient *Cp* for the fundamental frequency. Contour levels range from $10^{-10}$ (dark) to $10^{-4}$ (light) with the logarithmic scale.

backstep represents the source of the expansion waves, which are radiated from the vortices distorted in the wake of the backstep ($t=0.27\ T$ in Fig. 10).

### D. Phase distributions of vortices and acoustic waves

We investigated phase distributions Φ of the second invariant of the velocity gradient tensor and fluid density. Figure 14 shows the phase distributions along the observation line shown at the top for the fundamental frequency for $M=0.3$, 0.4, and 0.5. This observation line approximates the trajectory of the vortex because the amplitude of the second invariant fluctuations along this line takes its maximum in the wall normal direction (Fig. 15). The reference point is above the trailing edge of the backstep, and the phase of the second invariant at this point is the reference for both the phase distributions of the second invariant and those of fluid density.

The phase distributions of the second invariant represent the convection of the vortex, while those of the fluctuating density around the leading edge of the bump virtually represent the upstream propagation of the radiated sound waves because the density fluctuations caused by the convection of the vortices are negligibly small around this edge. Figure 14 shows that the phase of the second invariant coincides with that of the fluctuating fluid density at a downstream point of the leading edge of the bump. At this point, the compression waves cause the vortex formed by the flow separation at the leading edge of the bump to begin to stretch. The distance between this point and the leading edge of the bump is $L_\alpha \approx 5h$ for all the investigated Mach numbers.

The gradient of the phase distributions of the second invariant also gives the convection velocity of the vortices. We obtained the averaged convection velocity $u_{cb}=0.29u_0$ on the bump and $u_{c1}=0.19u_0$ from the trailing edge of the bump to the backstep. The convection velocity $u_{cb}$ on the bump is approximately confirmed by the trajectories of the vortices in Fig. 11. The vortices are convected very close to the wall, and the boundary layer is laminar. As a result, these vortices are strongly affected by the wall, and the convective velocities of these vortices are much slower than those of vortices in free shear layers such as deep cavities. Moreover, the phase distributions of the second invariant also show that the

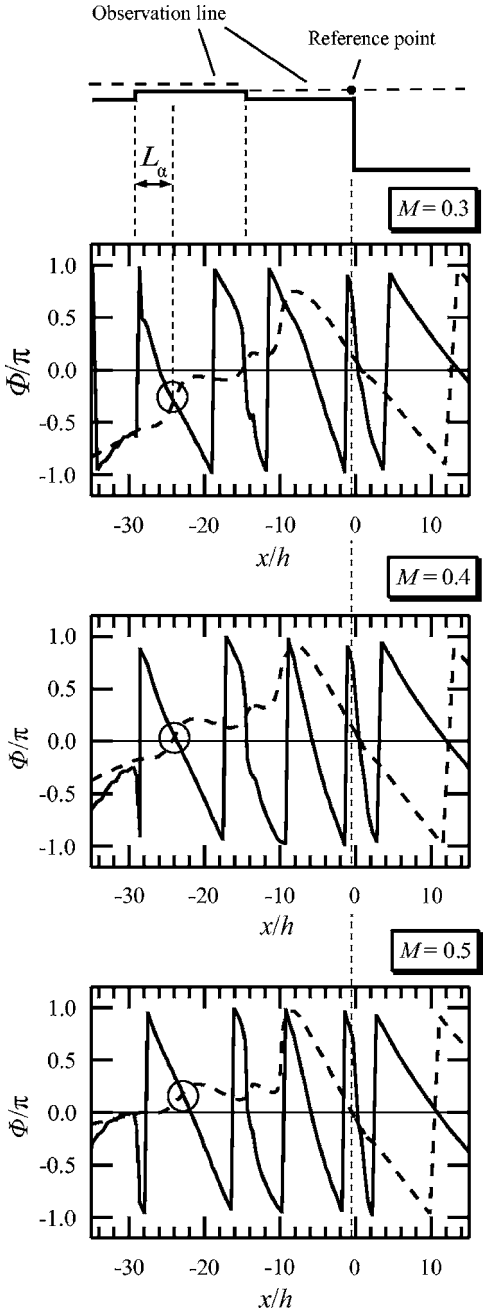


FIG. 14. Phase changes of second invariant (solid line) and fluctuating fluid density (dashed line) along the observation line for fundamental frequency.

distance between the vortex at the trailing edge of the backstep and its upstream vortex is very narrow. This is because one of the splitting vortices over the trailing edge of the backstep ("Vortex 1-2" in Fig. 10) is convected with a much slower velocity as already mentioned in Sec. III B. A compression wave is radiated between this slow vortex and its upstream vortex.

### E. Formula for frequencies of the tonal sound

The discussion so far focuses on the self-sustained oscillation mechanism and the phase relationship between the vortices and the acoustic waves. The cycle of the self-sustained oscillations consists of the following three parts:

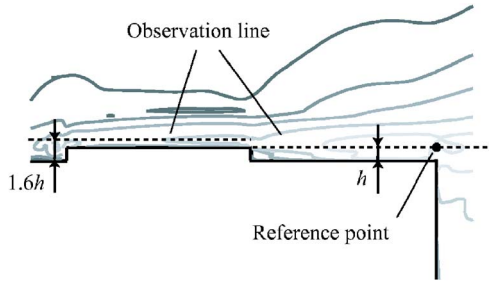


FIG. 15. Amplitudes of second invariant fluctuations $Q'/(u_0/h)^2$ near the bump. Contour levels range from $10^{-8}$ (dark) to $10^{0}$ (light) with the logarithmic scale. Dashed line (---) represents the observation line for phase investigation.

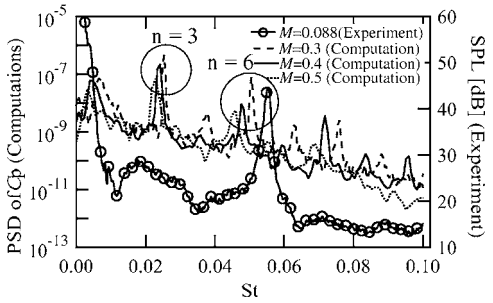


FIG. 17. Power spectrum density of pressure coefficient $Cp$ in computations compared with sound pressure level measured in experiment (circles are every tenth point).

(1) A small vortex is shed and begins to be convected at position $L_\alpha$ from the leading edge of the bump when a compression wave passes this point.

(2) The vortex is convected downstream at velocity $u_{cb}$ on the bump and $u_{c1}$ from the trailing edge of the bump to the backstep.

(3) The above-mentioned vortex splits into a fast vortex and a slow vortex when it passes the backstep. Between this slow vortex and its upstream vortex, a compression wave is radiated at position $L_\beta$ from the trailing edge of the backstep. This wave is propagated at a velocity of $a$-$u_0$ in the upstream direction.

The phase variation of the above processes must be $2\pi n$, where $n$ is a positive integer. As a result, the frequencies $f_n$ of the tonal sound can be predicted by the following formula:

$$f_n = 1/T_n,$$

$$T_n = ((L_b - L_\alpha)/u_{cb} + L_1/u_{c1} + (L_b + L_1 - L_\alpha - L_\beta)/(a - u_0))/n, \quad (4)$$

$$L_\alpha = 5.0h, \quad L_\beta = 3.6h, \quad u_{cb} = 0.29u_0, \quad u_{c1} = 0.19u_0.$$

To be exact, the point of the vortex shed is slightly different from the point of the isophase for $\rho$ and $Q$, when Fig. 14 is compared with Fig. 11. Therefore, we need to introduce the phase delay into this formula to predict the exact peak frequency. However, it is difficult to estimate the delay theoretically and the delay is not large (less than 10% of the fundamental period). The main objective of this paper is to clarify the self-sustained oscillations around the backstep with a bump and this simple formula is sufficient for this objective.

The frequencies predicted by this formula are compared with those measured in the experiments. As already mentioned, the backstep heights for the computational and the experimental configurations are different. We therefore estimated the effect of the backstep height on the radiated sound. Figure 16 compares the sound radiated from the original configurations with backstep height $H=21.6\ h$ with that from the configurations with $H=43.1\ h$. Figure 16 shows that the difference in the frequency spectrum is small. We concluded that the phenomena of the self-sustained oscillations around the bump do not depend on the backstep height as long as the backstep height is sufficiently larger than the bump height. Figure 17 compares the frequency spectra of the pressure fluctuations at the observation point in the computations with the sound pressure level measured by the microphone in the experiment. Mode $n=6$ is observed in both the experiment and the computations, but the lower mode, $n=3$, is only observed in the computations. We think this is because of the difference in Mach numbers. In fact, the amplitude of $n=3$ decreases and that of $n=6$ increases as the Mach number decreases in our computations. Also, Fig. 18 shows the changes in measured peak frequency for bump length $L_b$ where $M=0.088$ in the experiments. The predicted frequencies are in good agreement with those measured in the experiments. This agreement validates the self-sustained oscillation mechanism clarified by the present computational

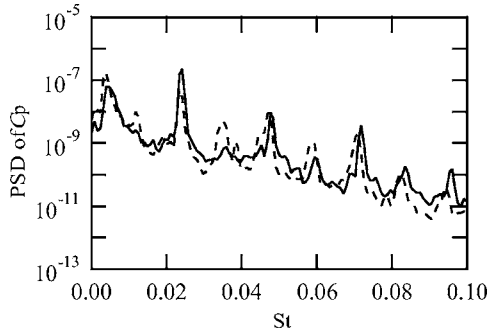


FIG. 16. Power spectrum density of pressure coefficient $Cp$ for baseline configuration (—) compared with that for the bump with a higher backstep (---).

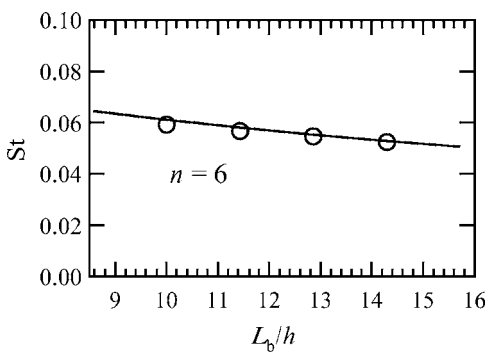


FIG. 18. Change in fundamental frequency for $L_b$. Fundamental frequencies predicted by Eq. (3) (—) are compared with experimental results (○).

study. In the present paper, we did not discuss the absolute values of the sound pressure level. For the quantitative prediction of the sound pressure level, it is necessary to exactly simulate the boundary conditions for both acoustic propagation and flow convection.

## IV. CONCLUSION

We numerically investigated flow structures and radiated sound in a flow over a backstep with a small upstream bump by directly solving the three-dimensional compressible Navier-Stokes equations. The results showed that a small vortex is shed from the leading edge of the bump and convected downstream to the backstep. When this vortex passes the backstep, it splits into a fast and a slow vortex. A compression wave is radiated between this slow vortex and its upstream vortex. Meanwhile, expansion waves are radiated from the vortices distorted in the wake of the backstep. The compression waves propagated toward the leading edge of the bump in turn shed new vortices by stretching the vortex formed by the flow separation at this edge. We also investigated the acoustic sources and the phase distributions of the second invariant of the velocity gradient tensor and fluctuating fluid density. As a result, we were able to identify the phase relationship between the vortices and the acoustic waves. Based on this relationship, we proposed a formula for predicting the frequencies of the radiated tonal sound. The frequencies predicted by this formula are in good agreement with those measured in the experiments. This agreement validated the present computational results.

The methods that we used to identify the phase relationship between the vortices and the acoustic waves in this paper are also useful for the clarification of other phenomena associated with fluid-acoustic interactions. Moreover, we believe that this clarification leads to an improved design guide for various industrial products for the suppression of the trouble caused by fluid-acoustic interactions discussed here.

[1] H. H. Heller and W. M. Dobrzynski, "Sound radiation from aircraft wheel-well/landing-gear configurations," J. Aircr. **14**, 768 (1977).
[2] O. W. Mcgregor and R. A. White, "Drag of rectangular cavities in supersonic and transonic flow including the effects of cavity resonance," AIAA J. **8**, 1959 (1970).
[3] G. B. Brown, "The vortex motion causing edge tones," Proc. Phys. Soc. London **49**, 493 (1937).
[4] A. Powell, "On the edge tone," J. Acoust. Soc. Am. **33**, 395 (1961).
[5] J. E. Rossiter, "Wind-tunnel experiments on the flow over rectangular cavities at subsonic and transonic speeds," Aero. Res. Counc. R&M, No. 3438 (1964).
[6] M. A. Kegerise, E. F. Spina, S. Garg, and L. N. Cattafesta, "Mode-switching and nonlinear effects in compressible flow over a cavity," Phys. Fluids **16**, 678 (2004).
[7] A. J. Bilanin and E. E. Covert, "Estimation of possible excitation frequencies for shallow rectangular cavities," AIAA J. **11**, 347 (1973).
[8] C. K. W. Tam and P. J. W. Block, "On the tones and pressure oscillations induced by flow over rectangular cavities," J. Fluid Mech. **89**, 373 (1978).
[9] D. G. Crighton, "The jet edge-tone feedback cycle; linear theory for the operating stages," J. Fluid Mech. **234**, 361 (1992).
[10] M. S. Howe, "Edge, cavity and aperture tones at very low Mach numbers," J. Fluid Mech. **330**, 61 (1997).
[11] L. Larcheveque, P. Sagaut, I. Mary, O. Labbe, and P. Comte, "Large-eddy simulation of a compressible flow past a deep cavity," Phys. Fluids **15**, 193 (2003).
[12] C. W. Rowley, T. Colonius, and A. J. Basu, "On self-sustained oscillations in two-dimensional compressible flow over rectangular cavities," J. Fluid Mech. **455**, 315 (2002).
[13] T. Colonius and S. K. Lele, "Computational aeroacoustics: progress on nonlinear problems of sound generation," Prog. Aerosp. Sci. **40**, 345 (2004).
[14] S. K. Lele, "Compact finite difference schemes with spectral-like resolution," J. Comput. Phys. **103**, 16 (1992).
[15] K. Matsuura and C. Kato, "Large-eddy simulation of compressible transitional flows in a low-pressure turbine cascade," AIAA J. **45**, 442 (2007).
[16] D. V. Gaitonde and M. R. Visbal, "Pad-type higher-order boundary filters for the Navier-Stokes equations," AIAA J. **38**, 2103 (2000).
[17] K. W. Thompson, "Time dependent boundary conditions for hyperbolic systems," J. Comput. Phys. **68**, 1 (1987).
[18] T. J. Poinsot and S. K. Lele, "Boundary conditions for direct simulations of compressible viscous flows," J. Comput. Phys. **101**, 104 (1992).
[19] J. W. Kim and D. J. Lee, "Generalized characteristic boundary conditions for computational aeroacoustics," AIAA J. **38**, 2040 (2000).
[20] J. B. Freund, "Proposed inflow/outflow boundary condition for direct computation of aerodynamic sound," AIAA J. **35**, 740 (1997).
[21] J. Larsson, L. Davidson, M. Olsson, and L. Eriksson, "Aeroacoustic investigation of an open cavity at low mach number," AIAA J. **42**, 2462 (2004).